JOURNAL OF PROPULSION AND POWER
Vol. 14, No. 3, May–June 1998

Model of Turbulent Mixing and Reaction for H_2–Air Combustion

Marc A. Cremer*
Reaction Engineering International, Salt Lake City, Utah 84101
Patrick A. McMurtry†
University of Utah, Salt Lake City, Utah 84112

A one-dimensional stochastic turbulent mixing model is formulated for application to a constant diameter, cylindrical combustion geometry. Simulations are performed to study effects of turbulence and nonequilibrium chemistry on NO formation in a cylindrically confined H_2–air jet. Effects of secondary air injectors, combustion tube diameter, flow rate, and equivalence ratio on NO formation are presented over a range of these parameters. It is illustrated that variations of these parameters can lead to reduced NO production by increasing the turbulence levels and through minimization of residence times in stoichiometric regions where NO production is greatest. Application of these results to the development of new burner concepts is addressed.

I. Introduction

THE simulation of turbulent reacting flows has attracted increased interest in recent years, particularly in an effort to increase combustion efficiency and decrease pollutant emissions. The need to improve efficiency is driven by the realization that fossil-fuel resources are continually decreasing. In addition, increased awareness of the environmentally damaging effects of pollutant emissions has sparked efforts to reduce the allowable limits of these emissions. Although the successes of turbulence models devised for and applied to nonreacting flows with constant fluid properties have demonstrated the feasibility of using predictive methods to solve these problems, in most cases, turbulent mixing models have had much difficulty in dealing with problems related to scalar transport and conversion in reacting flows. In particular, schemes used for the prediction of out of equilibrium chemical species in turbulent reacting flows have not been generally acceptable. Implementation of a mixing and chemistry model that realistically represents the coupling between the turbulence and chemistry is essential to accurately predict pollutant formation. The research results presented in this paper are specifically directed at this problem.

A. Motivation

Although the work presented here is of a fundamental nature, it was initially motivated by research in new burner concepts for advanced gas turbine engines for high-speed civil transport (HSCT). Under the direction of NASA, research in the U.S. on the HSCT has had a strong environmental focus with a top priority being the reduction of pollutant emissions from advanced gas turbine engines. Emissions of most concern are oxides of nitrogen (NO_x), carbon monoxide (CO), and all unburned hydrocarbons (UHC). In supersonic flight, it is believed that the emission of NO_x into the stratosphere is an important mechanism causing the depletion of ozone (O_3). NO and NO_2 can take part in a catalytic cycle in which ozone combines with atomic oxygen to form molecular oxygen while no NO_x is consumed. Under this mechanism, very small quantities of NO_x can destroy large quantities of O_3 (Ref. 1). CO and UHC are primarily formed during landing and takeoff operations when combustion efficiency is at a minimum. Investigations have shown that significant reductions in the quantity of CO and UHC formed in gas turbine combustors are obtainable with modifications of current technology or with modified methods of operating the combustors at idle. Reduction of NO_x emissions, however, has been more difficult and is regarded as the most formidable emission abatement technology challenge associated with gas turbine engines.[2]

Most data show that NO is the predominant nitrogen oxide emitted by combustion devices.[3] The two primary mechanisms of NO formation in the combustion of conventional fuels are the oxidation of atmospheric nitrogen (molecular) and the oxidation of nitrogen-containing compounds in the fuel (fuel nitrogen). In most combustion processes, molecular nitrogen is the dominant source of NO, although when high-nitrogen content fuels are used, formation of NO through fuel nitrogen pathways can be significant. Formation of NO in air-breathing combustors is favored in hot regions where free oxygen atoms are available.[4] Most experimental evidence indicates that maximum production occurs when the ratio of fuel to oxidizer is stoichiometric,[3,5] although some conflicting studies have indicated that maximum NO formation occurs in rich flame zones.[6] Drake et al.[3] argued that these measurements may have suffered from probe-sampling effects, which may explain their conflicting results.

Two main combustor designs have been identified for reducing emissions of NO_x. One design is the lean premixed prevaporized (LPP) combustor and another is the rich-burn quick-quench lean-burn (RQL) combustor. Of these two, the LPP design emits lower levels of NO_x but suffers from certain operational difficulties such as autoignition and narrow stability limits. The RQL design is more complex but does not suffer from the same difficulties as the LPP design. The RQL combustor incorporates dual stages, a fuel-rich primary stage and a fuel-lean secondary stage as illustrated in Fig. 1. Between the two stages is a quick quench zone in which the effluent from the primary stage mixes with secondary air prior to burning in the secondary stage. With this design, the existence of hot zones containing free-oxygen atoms is avoided. The primary zone is fuel rich, so that although the mixture is hot, there is a minimum of free-oxygen atoms. In the secondary stage, where there is an excess of O_2, the temperature is lower, reducing the formation of NO. It has been found that most of the NO is formed in the quick quench zone where effluent

Received Feb. 28, 1997; revision received Nov. 24, 1997; accepted for publication Nov. 25, 1997.

*Senior Engineer, 77 West 200 South, Suite 210.
†Associate Professor, Department of Mechanical Engineering.

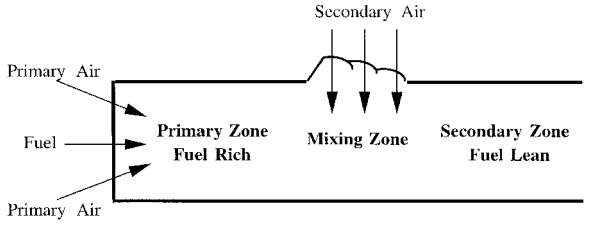

Fig. 1 Idealized illustration of the RQL combustor design.

from the primary stage combines with secondary air in an unsteady turbulent mixing process. The key to further reducing emissions in this low NO_x combustor design is to determine the best strategy for mixing the secondary air with the effluent from the primary stage to eliminate or significantly reduce the existence of stoichiometric zones within this region so that less NO_x is formed.

Experimental testing is needed to obtain reliable data concerning the effects of combustor design on engine emissions. However, performing experiments in conjunction with information gained through predictive methods based on knowledge of the relevant physical processes can substantially streamline the design process. In addition, once validated, numerical models constitute a tool that can be used to extrapolate beyond the experimental database to make predictions of performance for untested conditions.

B. Modeling Approaches

Most approaches used in simulations of reacting flows for design applications involve numerical solutions of the Reynolds-averaged Navier–Stokes (RANS) equations to determine the steady-state flow and thermochemical properties. Many predictive schemes developed for the solution of the RANS equations are based on gradient transport approaches for modeling the unclosed Reynolds stress and turbulent scalar flux terms.[7–9] Results obtained by these approaches indicate that gradient transport models are unable to adequately account for the unsteady nature of turbulent mixing because correlations between experiments and predictions deteriorate with increases in unsteadiness, particularly in predictions of pollutant formation.

The more promising approaches for dealing with chemical reactions make use of probability density function (PDF) methods.[10] These methods involve the determination of the joint scalar or joint scalar-velocity single-point PDF. Once this PDF is known, the mean chemical reaction rates appear in closed form. The difficulty with these methods lies within the determination of the single-point PDF. Two approaches are commonly used for this: 1) the general form of the PDF, parametrized by a few lower moments, is assumed, or 2) the PDF is determined by the solution of an evolution equation for the single point PDF. Although the benefits associated with these methods cannot be overstated, both approaches for determination of the PDF are problematic. With the assumed PDF method, the choice of the PDF shape is often quite arbitrary, and as the number of chemical species grows, this technique becomes limited by the number of first- and second-moment equations that must be modeled and solved. The direct PDF approach is more rigorous because the general form of the PDF is not assumed. However, its difficulties relate to how the unclosed molecular mixing terms are modeled in the solution of the single-point PDF. In most cases, variants of Curl's coalescence–dispersion (C–D) model are used.[11] It is widely recognized that these models have several fundamental shortcomings including the inability to distinguish between the distinct mechanisms of turbulent convection and molecular diffusion in turbulent scalar transport.

In this research, the linear eddy model,[12,13] a one-dimensional stochastic model of turbulent mixing, has been employed to model the turbulent reaction process. The key element of this model is the explicit incorporation of two distinct physical mechanisms in the turbulent mixing process: 1) turbulent convection and 2) molecular diffusion. Molecular mixing occurs through diffusive fluxes driven by local gradients of species concentration and, hence, is a small-scale effect. Turbulent convection reduces scalar length scales by means of compressive strain, thereby magnifying local gradients and accelerating mixing. The interaction of these processes at the smallest scales of the flow is difficult to capture using a modeling approach that does not differentiate between their unique effects. Multidimensional models cannot account for the small-scale spatial structure of the scalar field for realistic parameter ranges (because of computational limitations), and are thus incapable of accurately representing the combined effects of turbulent stirring and molecular diffusion.

The convection–diffusion–reaction equation governing the transport of a reactive scalar $\boldsymbol{\phi}$ in a turbulent flow can be expressed in the following form:

$$\frac{\partial \boldsymbol{\phi}}{\partial t} + \frac{\partial u_i \phi}{\partial x_i} = D_M \frac{\partial^2 \phi}{\partial x_i \partial x_i} + \dot{\omega} \tag{1}$$

where D_M is the molecular diffusivity. This equation expresses the effects of the two mechanisms governing turbulent mixing: (1) convection (stirring) of the scalar field by the velocity field, which results in the stretching and distortion of fluid elements; and (2) molecular diffusion, the mechanism by which scalar properties become mixed at the molecular level. The rate term $\dot{\omega}$ represents the rate at which ϕ is altered because of chemical reaction.

In the linear eddy model (LEM), the distinction among these different physical effects is retained by resolving all length scales of the flow. This is, of course, a computationally infeasible task in multidimensional flows. However, with a one-dimensional spatial description of the scalar field, complete resolution of the relevant range of length and time scales is achievable for flows with realistic Re.

Within this one-dimensional representation, molecular diffusion and chemical reaction are treated exactly through numerical solution of the diffusion–reaction equation

$$\frac{\partial \phi}{\partial t} = D_M \frac{\partial^2 \phi}{\partial x^2} + \dot{\omega} \tag{2}$$

A unique feature of the LEM, which allows for a physically plausible representation of turbulent mixing in one spatial dimension, is the manner in which turbulent convection is implemented. Convection is represented by randomly occurring rearrangement events that punctuate the diffusion-reaction process. Each event involves the instantaneous rearrangement of the scalar values within a randomly selected segment of the linear domain according to a specified rule.[13]

The complete modeling process is summarized as follows. Molecular diffusion and chemical reaction are treated as continuum processes acting on the scalar field and are treated in the model by numerical solution of the one-dimensional diffusion–reaction equation along the linear domain. Interrupting this process are randomly occurring rearrangement events. These events are governed by a Poisson process with mean rate $\boldsymbol{\lambda} B$, where B is the domain size and λ is a rate parameter with units $m^{-1}\ s^{-1}$. Note that λ can vary along the linear domain to represent spatial variations in turbulence intensity. The eddy size for each event is chosen by randomly sampling a PDF $f(l)$, which represents the eddy size distribution and its derivation is based on scaling laws for high-Reynolds number turbulent flows.[13]

Most relevant to the present work, the LEM was previously employed to predict pollutant formation in H_2–air combustion.[14] In that work a free H_2–air jet was treated. Empirically derived entrainment laws were used to treat the secondary air

Table 1 Ten-step H_2–air chemical mechanism

Reaction	A_j	b_j	E_j	Reaction step
$H + O_2 = OH + O$	1.2×10^{17}	−0.91	69.1	(R1)
$O + H_2 = OH + H$	1.5×10^{7}	2.0	31.6	(R2)
$OH + H_2 = H_2O + H$	1.0×10^{8}	1.6	13.8	(R3)
$OH + OH = H_2O + O$	3.4×10^{13}	0.0	21.0	(R4)
$H + HO_2 = OH + OH$	1.5×10^{14}	0.0	4.2	(R5)
$H + OH + M = H_2O + M$	2.15×10^{22}	−2.0	0.0	(R6)
$H + H + M = H_2 + M$	1.83×10^{18}	−1.0	0.0	(R7)
$O + O + M = O_2 + M$	2.86×10^{18}	−1.0	0.0	(R8)
$H + O + M = OH + M$	6.2×10^{16}	−0.6	0.0	(R9)
$H + O_2 + M = HO_2 + M$	2.0×10^{18}	−0.8	0.0	(R10)

entrainment into the fuel jet,[15] and finite rate chemistry was implemented using a mechanism for H_2–air combustion that was previously developed by Chen and Kollman.[16] A thermal mechanism for NO production was added using the extended Zeldovich mechanism.[17]

The simulations in that work were performed for a fuel consisting of 22% argon–78% hydrogen reacting with air. This particular fuel was chosen so that comparisons with the experimental results of Magre and Dibble[18] and the PDF computations of Chen and Kollman[19] could be made. Menon et al.[14] noted close agreement with the experimental results, particularly in scatter plots of temperature T vs mixture fraction ξ illustrating the coupling between the finite rate chemical kinetics and the turbulence. Also, the linear eddy predictions of the NO emission index (EI_{NO}), with units g NO/kg H_2, compared very well with the PDF computations. Other qualitative trends of the dependence of NO production on fuel velocity and on temperature and radical concentrations were also found to be consistent with experimentally measured trends.

C. Current Problem Configuration

The combustion geometry treated here is that of a confined jet in a constant diameter cylindrical geometry. The fuel jet passes through a confined cylindrical region into which specified quantities of air are injected at specified locations and rates. This geometry allows for an investigation of the effects of injection strategies on the rate of mixing between the air and fuel and on the rate of production of NO. Although notably simplified from the actual combustion chamber of a gas turbine combustor, this geometry is suitable for the mixing region in the RQL combustor, where partially reacted fuel and combustion products mix with specified quantities of secondary air.

The remainder of this paper is divided into four sections as follows. The reduced chemical mechanism for H_2–air combustion is discussed in Sec. II. Section III provides a detailed description of how the primary components of the model, turbulent mixing, chemical reaction, and the various application specific processes dealing with streamwise fluid motion and injection, are assimilated in the current implementation. In Sec. IV, model predictions of the effects of various parameters on the statistics of the mixture fraction and temperature as well as on NO and other species concentrations are discussed. Section V provides a final summary and assessment of the work.

II. Chemical Mechanism

Conceptually, any finite rate kinetics mechanism could be implemented within each computational cell of the linear eddy mixing model to account for chemical species production and destruction. This is accomplished by solving an additional diffusion–reaction equation within each cell for each chemical species. Such mechanisms could be general enough to account for differences in thermal and molecular diffusivities and include large numbers of species and many elementary reaction steps. To improve the computational efficiency, models often incorporate simplifications of the actual full chemical mechanism.

The mechanism used in this research is a reduced H_2–air mechanism developed by Chen and Kollman.[16] For a nonpremixed H_2–air jet flame, they considered the 10 elementary reactions shown in Table 1. The rate constant for the jth reaction is given by $k_j = A_j T^{b_j} \exp[-E_j/(RT)]$, and the values A_j, b_j, and E_j are obtained from Warnatz.[20]

Beginning with a set of 10 scalars, which are the seven active chemical species (H_2, O_2, H_2O, O, H, OH, and HO_2), plus temperature, density, and pressure, assuming equal diffusivities for all species and temperature, constant pressure (this is usually assumed in gas turbine combustion chambers), the ideal gas law, and that the bimolecular reactions R1–R5 in Table 1 are very fast compared to the three-body radical recombination reactions R6–R10, the total number of scalars describing the combustion process of Table 1 can be reduced to two. These are a conserved scalar variable ξ and a reactive scalar n. For H_2–air combustion, ξ is the mass fraction of H atoms normalized so that $\xi = 1$ in the fuel stream and 0 in the oxidizer stream. Using this definition, the concentrations of the atomic species and the mixture enthalpy are linearly related to ξ. Following the work of Chen and Kollman,[16] the reactive scalar (progress variable) n that is used in this work is the total number of species moles per unit mass (kmoles/kg).

An additional mechanism must be implemented to predict the formation of NO. In the general case of a hydrocarbon flame, NO can be formed through three different pathways: 1) thermal NO, 2) prompt NO, and 3) fuel NO. In the case of clean fuels (fuels not containing nitrogen compounds), fuel NO is not formed. Prompt NO is formed through a mechanism involving a HCN intermediate and is important in hydrocarbon flames.[21] For an RQL burner in which conventional hydrocarbon fuels are used, the formation of NO_x precursors such as HCN, in the rich zone, would be of concern. However, for the hydrogen flame that is considered in this work, only the thermal NO pathway is important and is described by the extended Zeldovich mechanism. Upon assuming a steady state for the N atom concentration and that [NO] is well below its equilibrium value, the extended Zeldovich mechanism can be reduced to the single global step[4,7]

$$N_2 + O_2 = 2NO \tag{3}$$

and the NO formation rate (g/cm^3 s) can be approximated as $S_{NO} = 2k[N_2][O]M_{NO}$, where $k = 1.84 \times 10^{14} \exp(-38{,}370)/T$ cm^3/mol-s and [ ] denotes concentration given in (mol/cm^3). Note that the NO formation rate is very sensitive to temperature as can be seen by the relatively large negative value for the activation energy. It is also important to point out that the rate depends on the oxygen atom concentration rather than the concentration of oxygen molecules. Assuming that O and O_2 are in equilibrium can lead to significant underprediction of the rate of NO formation because relatively high superequilibrium concentrations of O can exist in diffusion flames.

An important point that should be made here is the applicability of the chosen reduced mechanism in treating the problem of thermal NO formation. The reduced mechanism is

based on high-temperature combustion of H_2 with air and the assumptions of partial equilibrium are valid near the stoichiometric point where temperatures are high. Because thermal NO is formed at high temperatures, above 1800 K, the reduced mechanism is a reasonable representation for studying NO in hydrogen combustion.

Coupling the reduced H_2–air reduced mechanism with the extended Zeldovich mechanism results in a total of three scalar equations that need to be solved: 1) mixture fraction, 2) progress variable, and 3) NO concentration. In the context of the linear eddy solution methodology, these equations are

$$\rho \frac{\partial \xi}{\partial t} = \frac{\partial}{\partial x}\left(\rho D \frac{\partial \xi}{\partial x}\right) \tag{4}$$

$$\rho \frac{\partial n}{\partial t} = \frac{\partial}{\partial x}\left(\rho D \frac{\partial n}{\partial x}\right) + \left[\frac{\mathrm{d}n}{\mathrm{d}t}\right]_{\xi,n} \tag{5}$$

$$\rho \frac{\partial n_{\mathrm{NO}}}{\partial t} = \frac{\partial}{\partial x}\left(\rho D \frac{\partial n_{\mathrm{NO}}}{\partial x}\right) + \left[\frac{\mathrm{d}n_{\mathrm{NO}}}{\mathrm{d}t}\right] \tag{6}$$

where ρ is the mixture density, n is the progress variable with units kmole/kg, and n_{NO} is the NO progress variable with units kmole NO/kg. The mixture fraction describes the extent of mixing while the progress variable embodies information concerning the extent of chemical reaction. Knowledge of these two values alone allows for the determination of all remaining unknown species concentrations, density, and temperature. The source term in Eq. (5) is obtained from the look-up table produced by solution of the reduced mechanism. Neglecting the equation for the progress variable is equivalent to ignoring effects of finite rate kinetics. For example, knowledge of the mixture fraction alone would be sufficient to compute equilibrium species concentrations, density, and temperature.

III. Implementation

The mixing region of the RQL combustor treated here includes a confined cylindrical region with downstream ports to accommodate air injection. A simple schematic of the computational configuration is shown in Fig. 2.

Fuel enters the combustor at the inlet on the left at a temperature of 300 K, while air is injected at multiple locations downstream, also at a temperature of 300 K. The linear eddy domain is taken to be along the centerline of the combustor and extends some appropriate number of diameters N_d downstream. The N_d diameters or blocks are further divided into N_c equally spaced cells of width $\Delta x = L/N_c N_d$, where L is the length of the linear eddy domain. This degree of resolution is determined to be sufficient if a factor of 2 increase in N_c produces no apparent change in the scalar properties. For the simulations discussed here, N_d ranged from 10 to 40 and N_c ranged from 200 to 800.

Because the LEM is strictly a turbulent scalar mixing model, velocity field statistics are not predicted outputs. To account for the bulk fluid motion in the streamwise direction caused by air injection, fuel feed, and thermal expansion, a distinct computational step must be implemented. The first two contributions to streamwise flow reflect an introduction of mass at constant density while the third reflects reduction of the reacted fluid density at constant mass. All three, however, represent volume sources. In the case of air injection and fuel feed, the volume of the affected cell is first held constant, causing an intermediate increase in density. In the case of thermal expansion, the intermediate cell density remains unchanged, so that upon volume expansion the fluid density will decrease. When the fuel feed, air injection, and combustion processes are completed at the end of a diffusion time step, the intermediate cell densities are compared with their equilibrium values, computed based on the ideal gas law assuming constant pressure. To reconcile the volumes, cell contents are transferred to downstream locations so that the cumulative equilibrium volume from (0, x) matches the cumulative cell volume over the same range.

In the case of air injection, the result of the expansion routine is as shown in Fig. 3 in which a parcel of air of finite size L_i is injected into the domain at location x_i. The size of the injected air parcel is an important input parameter and is physically related to the size of the injector. If the size L_i of the injected air parcel and the overall equivalence ratio are known, the mean rate of air injections $\bar{\tau}_i$ at location x_i can easily be determined. Fuel in-flow is modeled in a similar manner in which fluid of a volume equivalent to that of the incoming fuel is instantaneously displaced downstream. Accounting for thermal expansion, however, is not so straightforward, and the method as described earlier is accomplished on the discretized domain as directed by Kerstein.[15] The implementation of this process must be carried out carefully to avoid the occurrence of numerical diffusion caused by spurious mixing of neighboring cells. Inaccuracies caused by this effect can be the most severe in the case of high Sc fluids.

Time steps for diffusion, reaction, stirring (rearrangement events), fuel feed, and air injection, are key parameters in the implementation of the model and are each specified as follows. The diffusion time step τ_d is determined to guarantee numerical stability of the solution of the one-dimensional diffusion equation. This constraint requires $\tau_d = (\Delta x)^2/D_m C$, where $C \geq 2$ and $D_m = \nu/\mathrm{Sc}$. Sutherland's law is used to provide an estimate of the variation of dynamic viscosity μ with temperature. The

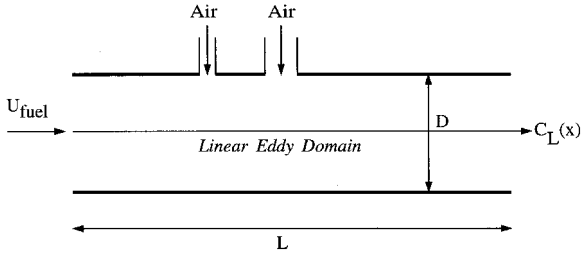

Fig. 2 Schematic of the configuration used for linear eddy modeling of the mixing region in the RQL combustor.

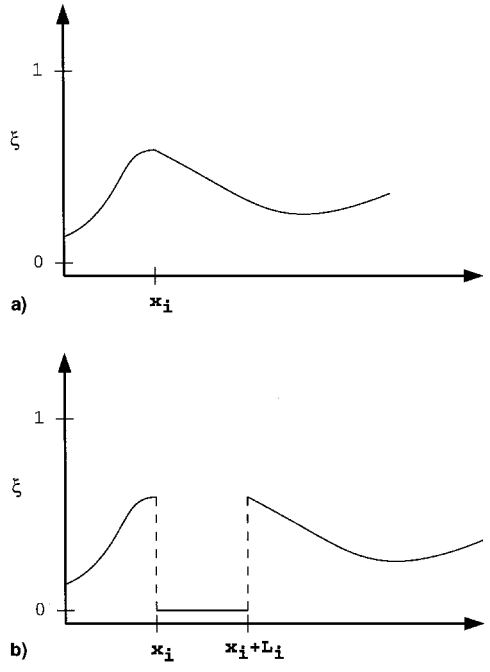

Fig. 3 Illustration of the model process of air injection at a downstream location x_i. Centerline value of the scalar a) prior to air injection and b) after injection of a volume of air represented by L_i.

kinematic viscosity ν is then computed as $\nu = \mu/\rho$. The chemical rate terms, dependent on the reduced mechanism, are computed in time steps corresponding to the diffusion time step of the simulation. These rates along with species data are tabulated beforehand in a separate solution of the reduced mechanism. The stirring time step τ_s is computed using the rate parameter λ, as previously described. Local values of λ are dependent on the local turbulence intensity and are computed for each block based on a locally determined $Re = VD/\nu$. A global event rate $E(t)$ is obtained by integrating $\lambda(x, t)$ over the entire domain of length L. The overall stirring time step is then given by computing the inverse of $E(t)$. The time step for fuel injection is taken to be the same as the diffusion time step. The injector time step τ_i is taken to be the minimum of the $\tau_{i,j}$, defined to be the time step to the next scheduled injection at injector j. The $\tau_{i,j}$ are each sampled from an exponential distribution with mean time $\bar{\tau}_{i,j}$. This procedure is carried out to model the injection step as a Poisson process.

A simulation begins by initializing the model parameters and the scalar fields. Initial time steps for diffusion, stirring, and injection are computed. Based on the relative sizes of these time steps, the simulation proceeds so that each of these processes progresses at the desired frequency.

When the epoch for a stirring event is reached as determined by t_s, a rearrangement event is carried out. A position for the event center is selected randomly within a block. The block is selected in a manner that favors those having large local λ by sampling a position x from the PDF defined by $\lambda(x, t)/E(t)$. Thus, the variation in local Re within the domain directly affects the spatial variation of $\lambda(x, t)$ and influences the variation in turbulence intensity within the model. The size of the eddy is selected according to the PDF $f(l)$ defined in Sec. I. The mapping process is then accomplished by permuting the scalar values over the affected region according to a specified mapping rule.[13] A new stirring time t_s is then updated and this process is repeated when $t = t_s$.

When the epoch for air injection at any of the injectors is reached, the desired quantity of air is injected at the selected location in the manner shown in Fig. 3. After completion of the injection, a new time step $\tau_{i,j}$ for the affected injector is determined, and $\tau_i = \min_j[\tau(i, j)]$ is computed. The next injection time t_i is then determined and the injection process is repeated when $t = t_i$.

In a similar manner, when the epoch for diffusion is achieved, the mixture fraction, progress variable, and the NO concentration are updated in each cell. Additional fuel is introduced at the inlet and the expansion process is carried out. Based on the new properties within the linear eddy domain, local values of the Re are computed and a new stirring time step τ_s is determined. Meanwhile, statistics for the scalar field properties are accumulated following an initial transient period. The simulation proceeds for the period t_f so that statistics of the steady-state process (independent of the initial conditions) are suitably converged.

IV. Model Predictions

The overall objective of these simulations was to determine how changes in parameters of the mixing and reaction process affect NO formation in a geometry relating to the mixing region in the RQL combustor. Although the physical processes occurring in the mixing region are, in general, three dimensional and complicated by features that are not considered in this simplified approach, this implementation can be effectively utilized to investigate fundamental effects of changes in velocity and length scales and how these changes couple with finite rate kinetics in the framework of inertial range turbulence. Based on previous model applications to reacting and nonreacting flows,[12–15,22–25] and the ability of the model to correctly predict scaling properties, a large body of literature exists providing confidence in the trends shown next.

The fuel used to obtain the majority of the model results was a mixture consisting of 78% H_2 and 22% Ar. This particular fuel mixture has been used in both experimental[18] and computational,[14,19] diffusion flame studies. Some simulations were also performed for the case of an undiluted hydrogen flame for comparison. Statistics of the mixture fraction, progress variable, temperature, density, and species concentrations were gathered for a large number of simulations. The NO emission index EI_{NO}, defined as the cumulative gram mass of NO produced per kg mass of fuel entering the combustor, was also computed and used as the primary parameter indicating the extent of NO emission. Mixing and reaction variables that were considered were the equivalence ratio, fuel dilution, fuel velocity, combustor diameter, and several injector variables. These included injector locations, sizes, and relative flow rates. Statistics were gathered by first allowing the simulation to come to a statistical steady state so that effects of the initialization were no longer apparent. The initial transient period was defined to be the mean time required for a fluid particle to traverse the entire length of the combustor assuming a velocity equal to that of the incoming fuel. Instantaneous snapshots of the flowfield properties were then accumulated over time to compute time averages as well as variances and higher-order statistics. Particular attention was placed on the mixture fraction and temperature as well as species concentrations.

For the H_2–Ar case, stoichiometric values of the mixture fraction and equilibrium progress variable are $\xi_{stoi} = 0.1636$ and $n_{stoi} = 0.0388$ kmoles/kg, and the adiabatic flame temperature is approximately 2320 K. For the pure H_2 case, these values are $\xi_{stoi} = 0.0283$ and $n_{stoi} = 0.0412$ kmoles/kg with an adiabatic flame temperature of approximately 2390 K. All predictions that are shown for this configuration will be discussed in terms of a baseline simulation whose parameters are as shown in Table 2.

The mixture fraction is an important indication of the extent of mixing. Figure 4 shows the predicted variation of the mixture fraction with axial position and the effects of changing the injector length scale and fuel velocity. The mean mixture fraction drops from a value of 1 at the inlet to the fully mixed value of approximately 0.115, corresponding to a mixture that is fuel lean. The snapshot of the mixture fraction at one instant shows that large fluctuations exist in the vicinity of the injector at $x/D = 1$. Parcels of air having a mixture fraction value of 0 are being injected at this location. A comparison of Figs. 4a and 4b clearly shows that the rms decays faster in the case of finer injection length scales. Comparison of Figs. 4a and 4c shows that although the rms appears to decay more slowly in Fig. 4c when plotted vs axial position, mixing actually proceeds more quickly in time in this case because of the higher turbulence intensity.

Plots of the fourth normalized moment, the kurtosis, for the same three cases are shown in Fig. 5. In all three cases, the kurtosis appears to first rise sharply in the vicinity of the injector and then decay to its Gaussian value of 3 further downstream, where it remains constant. This indicates that the PDF of the mixture fraction can be approximated as Gaussian in the limit of decreasing rms. This prediction is in agreement with experimental results obtained for several different tube geometries.[26] It has also been noted that Gaussian shapes are

Table 2 Simulation baseline properties

Parameter	Value
Diameter, cm	8
Number of injectors	1
Injector location (x/D)	1
Injection size, L	$0.02D$ (0.16 cm)
Fuel composition	78% H_2 22% Ar
Fuel velocity, m/s	10
Jet Reynolds number	41,386
Equivalence ratio	0.67

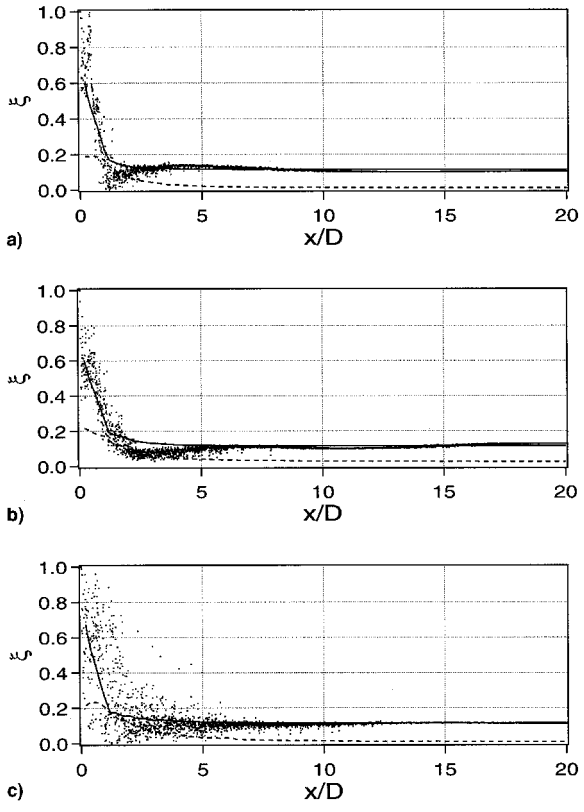

Fig. 4 Instantaneous (·····), mean (——), and rms (– – –) values of the mixture fraction showing effects of injector size and fuel velocity: a) baseline case, b) injector length $L_i = D/5$, and c) fuel velocity $U = 20$ m/s.

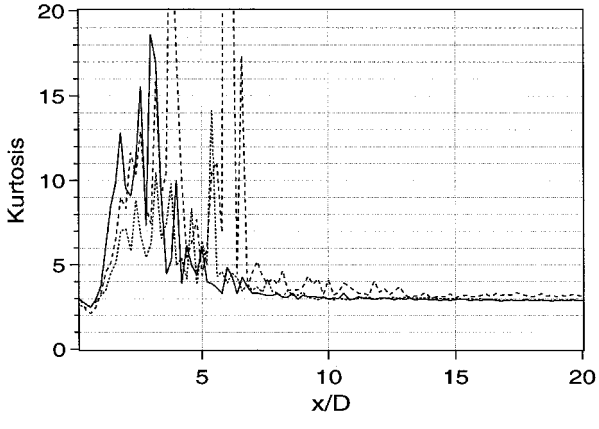

Fig. 5 Evolution of the fourth normalized moment (kurtosis) for the same cases as shown in Fig. 4. Baseline case (——), injector length $L_i = D/5$ (---), fuel velocity $U = 20$ m/s (– – –).

to be expected in light of the central-limit theorem.[27] This result gives some justification for the use of Gaussian and clipped-Gaussian single-point scalar PDFs in assumed PDF models of turbulent mixing.

The interaction between the chemistry and turbulence is best seen in predictions of the temperature and species scalar fields. Because many combustion models assume that time scales of the combustion reactions are fast in comparison to the mixing time scales, they often incorporate equilibrium chemistry. It is therefore instructive to compare predictions obtained assuming finite rate chemistry using the previously described reduced mechanism for H_2–air, with those obtained assuming equilibrium chemistry. Figures 6 and 7 show the axial variation of temperature and species concentrations for both cases. It can be seen in Fig. 6 that agreement is good for temperature and the major species H_2O, O_2, and H_2. The differences are greatest

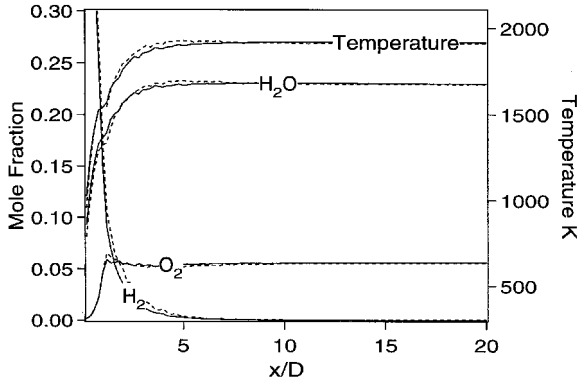

Fig. 6 Axial variation of temperature and species mole fractions comparing the effects of finite rate chemistry (——) with the assumption of chemical equilibrium (– – –) for the baseline case of Table 3.

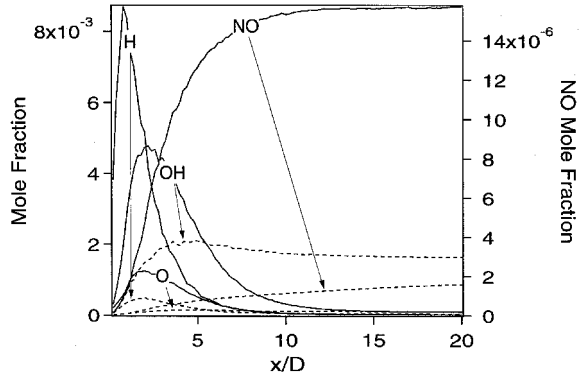

Fig. 7 Axial variation of O, OH, H, and NO mole fractions for the same cases as in Fig. 6. ——, finite rate chemistry, – – –, chemical equilibrium.

in the high-intensity mixing region near the injector, but become negligible further down the length of the combustor where equilibrium conditions exist. However, a comparison of radical species concentrations indicates a much different picture. Predictions of O, OH, H, and NO concentrations shown in Fig. 7 indicate that the assumption of chemical equilibrium leads to significant underprediction of these species in the high-intensity mixing region. As described by the extended Zeldovich.[17] mechanism, an underprediction of O atom concentration leads to a reduced rate of NO formation. It can be seen that most of the NO is being formed in the region where superequilibrium concentrations of O atoms exist. Very little NO is produced when the O atom concentration drops to its equilibrium value.

Another way to illustrate the existence of superequilibrium radical concentrations is to compute species concentration as a function of mixture fraction ensemble averaged over the domain. Under the assumption of equilibrium chemistry, the mixture fraction uniquely defines each species concentration, temperature, and density. In the framework of the H_2–air reduced mechanism, both the mixture fraction and the reaction progress variable are necessary inputs.

Figure 8 shows the same data as Fig. 7 plotted in this manner. Figures 8a and 8b show the effect of fuel velocity and nonequilibrium chemistry on combustion temperature and O atom concentration, respectively. Nonequilibrium effects are most significant in the vicinity of the stoichiometric mixture fraction where the flame temperature and O atom concentration are the highest. Increased jet velocities consistently produce larger superequilibrium O atom concentrations leading to lower average flame temperatures.

An explanation of the increased effects of superequilibrium with increasing jet velocities can be based on a Damköhler

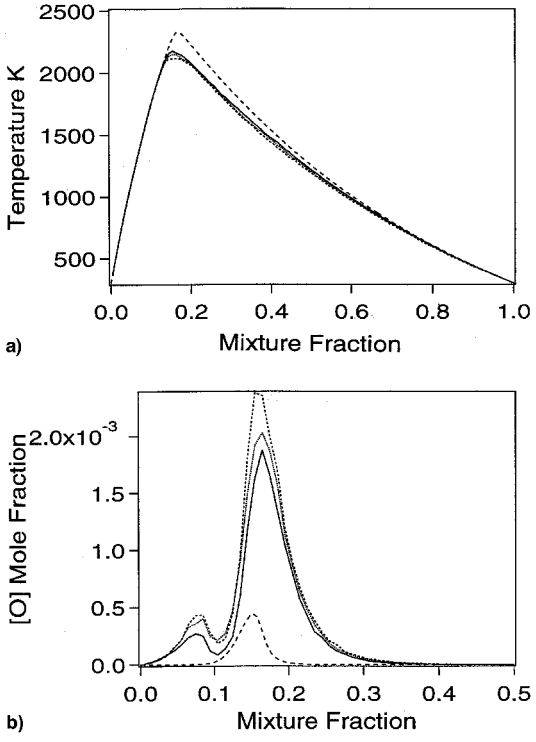

Fig. 8 Comparisons of chemical equilibrium (- - -) with finite rate chemistry (all other lines). Baseline case with U = 10 m/s (——), U = 20 m/s (· · · · ·), and U = 40 m/s (----): a) temperature and b) O mole fraction.

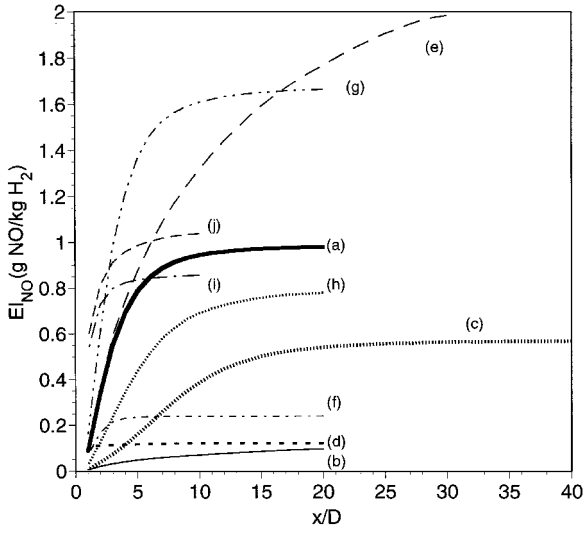

Fig. 9 NO emission index: a) baseline case; b) chemical equilibrium; c) U = 40 m/s; d) premixed fuel and air; e) injector length $L_i = 0.2D$ (1.6 cm); f) equivalence ratio = 0.5; g) undiluted H_2; h) D = 0.16 m, $L_i = 0.01D$ (0.16 cm), i) U = 20 m/s; and j) D = 0.16 m, $L_i = 0.02D$ (0.32 cm).

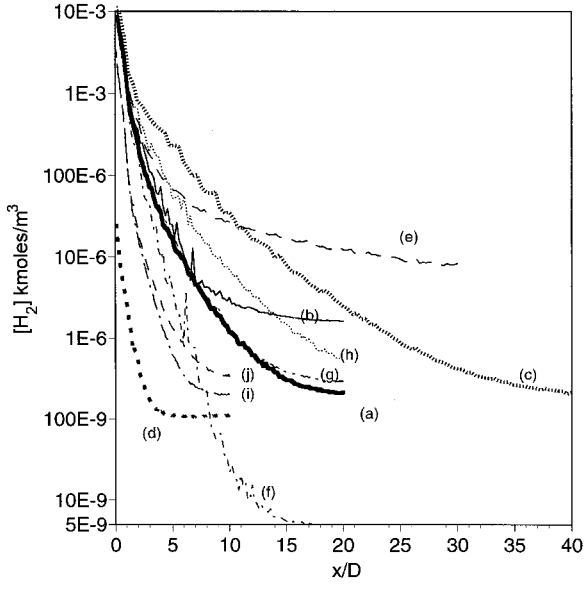

Fig. 10 Axial variation of H_2 concentration for same labeling and cases as Fig. 9.

number (ratio of characteristic mixing and reaction time scales) analysis. As the jet velocity increases, the turbulence intensity increases causing a reduction in the overall mixing time scale while the reaction time scale is unchanged. Taking the reaction time scale to be representative of the time scales for the three-body radical recombination reactions, increasing jet velocities cause the mixing time scale to become more competitive with the reaction time scales. This causes a larger departure from chemical equilibrium as is seen in the predictions of Fig. 8. This observation is entirely consistent with experimental data obtained for turbulent, nonpremixed, H_2–air flames obtained by Barlow et al.[28] These and other observations play a significant role in thermal NO production. As shown in Fig. 7, assumption of equilibrium concentrations of the radical concentrations results in significant underprediction of the rate of formation of NO. It is also apparent from Fig. 8 that mixing effects such as fuel velocity play a role in the extent of departure from chemical equilibrium, and will likely have an effect on NO formation.

Figure 9 shows the predicted effect of a number of mixing and chemistry parameters on thermal NO formation in this combustor configuration. Here, NO production is measured in terms of the NO emission index EI_{NO}. EI_{NO} is defined as the number of grams of NO produced per kilogram of H_2 entering the combustor. It can be observed in Fig. 9 that for the cases shown, EI_{NO} rises from a value of 0 at the inlet and plateaus to a relatively constant value some distance downstream. The rate at which this occurs depends very strongly on the temperature and O atom concentration. Because the definition of EI_{NO} is based on the weight of unreacted fuel entering the inlet, valid comparisons are obtained by determining EI_{NO} at locations where the concentration of remaining H_2 is approximately the same low value. In consideration of this, Fig. 10, which shows the variation of the concentration of H_2, should be closely considered when comparing EI_{NO} in Fig. 9.

Figures 9 and 10 indicate that in all cases, except for the increased injector size $L_i = D/5$, a plateau in the curves has been reached. In this particular case, the combustion is mixing limited because of the large injection length scales. At a location of x/D = 30, a significantly higher concentration of H_2 remains than in the remaining cases, and NO continues to be produced. In these remaining cases, EI_{NO} and [H_2] have reached plateaus at this position, indicating that additional NO is not being produced downstream of this location.

The effects of parametric changes can be best observed by comparison to the baseline case whose properties are listed in Table 2. As discussed previously and shown in Fig. 9, assumption of equilibrium concentrations of radical concentrations for computation of NO formation results in underpredictions. Premixing the fuel and air at the inlet produces very little NO. The primary reason for this is that regions containing stoichiometric mixtures of fuel and oxygen, where most of the NO is produced, are entirely avoided because the overall equivalence ratio here is 0.67. Making the combustion chemistry increasingly fuel lean further reduces NO production because of the lower overall temperatures that exist in nonstoichiometric mixtures. Increasing the jet velocity also has the effect of producing lower levels of NO. At first, this obser-

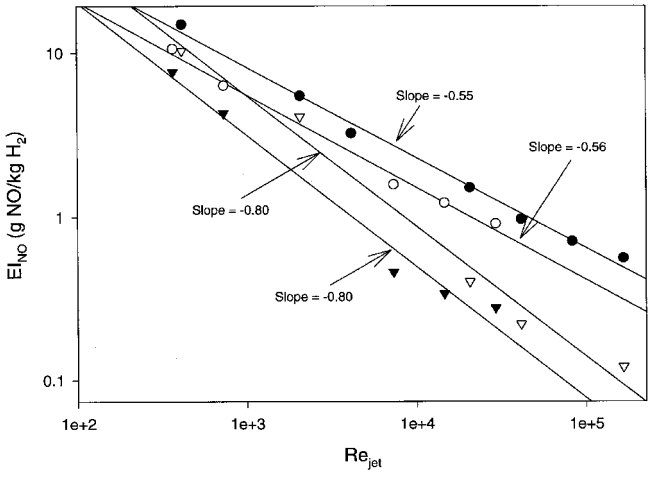

Fig. 11 Effect of jet Reynolds number on the formation of NO measured by the emission index. The lines are from least-square curves fits with the predicted slopes shown. The cases shown are combinations of two equivalence ratios, ϕ, with either diluted (78% H_2 22% Ar) or undiluted (100% H_2) fuel: ϕ = 0.67, diluted (○); ϕ = 0.5, diluted (▲); ϕ = 0.67, undiluted (●); ϕ = 0.5, undiluted (△).

vation appears to be in contradiction to Fig. 8b, which indicates the existence of higher concentrations of O atoms in this case. However, the increased velocities enhance mixing as a result of the higher turbulence intensity. The effect of this is to minimize stoichiometric regions where the temperatures and radical concentrations are the highest. Thus, the overall residence time within these regions is lower, resulting in lower NO production. The same is true when the jet diameter is increased (Fig. 9, curve i) illustrating that the NO emission has a clear *Re* dependence. Increasing the jet diameter and the injector length scales in the same proportion has little effect on the NO emission index (Fig. 9, curve j). For the case of increased injector length scales with fixed jet diameter, mixing is less efficient, resulting in increased NO production. The effect of fuel dilution can be seen by comparing the baseline case with the pure H_2 case. This is entirely a chemistry effect in that when the fuel is not diluted with Ar, the combustion temperature is higher, causing an overall higher rate of NO formation.

Further analysis of the effect of jet *Re* on the EI_{NO} indicates that a power-law scaling exists as shown in Fig. 11. The value of EI_{NO} that is plotted for each case is the plateau value as seen in Fig. 9. The model predicts two different scalings depending on the air–fuel mixture. Fuel dilution is not predicted to affect the overall scaling, but does affect the level—primarily a result of the different temperature levels that exist for different fuel dilutions. These predictions appear to be in general agreement with experimentally obtained scalings between EI_{NO} and *Re* obtained by Bilger and Beck,[29] Peters and Donnerhack,[30] and Chen and Driscoll[31] for the case of a jet diffusion flame with and without coaxial air.

V. Conclusions

A one-dimensional stochastic model has been formulated to study effects of mixing strategies on NO formation in a confined H_2–air jet. Reducing the description of the scalar field to one dimension allows resolution of turbulent stirring, molecular diffusion, and chemical reaction down to the smallest scales of the flow. This resolution is necessary to provide realistic predictions of the coupling between fluid mechanics and chemistry that govern the chemical conversion rates of secondary species in the H_2–air flame. Configuration specific processes, including the fuel and secondary air injection, and thermal expansion have been accounted for in a physically reasonable manner within the one-dimensional formulation.

The results of this modeling effort have provided information on effects of various design parameters on mixing and reaction in a combustion geometry representative of an RQL combustor. Although no data exist for direct comparisons, results of previous linear eddy mixing and reaction simulations have served both to validate aspects of the model and to provide mechanistic interpretations of measured properties in a unifying framework. Comparisons of the trends revealed by the present study with similar combustion configurations provide confidence in the trends of NO formation on various adjustable parameters. In this regard, the data are most useful in considering effects of different combustor design changes on the effects of NO in H_2–air combustion.

The present results illustrate how modifications in residence times (changing mean flow rates through geometry or mass flow variations), temperature (fuel stoichiometry), and temperature distributions (secondary fuel injection) all affect product formation by modifying the instantaneous radical concentrations. In particular, a scaling was shown in which NO emission index exhibited a power-law decrease with increasing jet Reynolds number. The decrease was described to be a result of higher turbulence levels and lower residence times at stoichiometric mixtures. The magnitude of the emission index was shown to be dependent on fuel dilution, but the rate of decrease with increasing Reynolds number, for a given equivalence ratio was not. Lowering the equivalence ratio resulted in both lower values of the emission index (because of lower temperatures) and a faster decrease with increasing Reynolds number. Increasing injector length scale resulted in an increase in the NO emission index as conversion of H_2 became mixing limited and higher concentrations of H_2 remained further downstream. Premixing results in very small amounts of NO being formed if the mixture is at an equivalence ratio less than one. This is a result of the complete avoidance of regions of stoichiometric mixtures. This latter observation is the motivation behind lean premixed prevaporized (LPP) combustion processes, but stability and autoignition issues remain a key issue here.

Although multidimensional calculations are more desirable for specific design applications, the resolution required to accurately simulate the turbulent mixing and chemical conversion would be computationally infeasible. As such, the current methodology provides a unique tool to be used in conjunction with experiments and multidimensional calculations for the design of advanced combustors. The model can be used in a stand-alone framework as discussed in this work, but also can be coupled with multidimensional, steady-state simulations.[32]

Acknowledgment

This work was funded by the National Science Foundation under Grant CTS 92-58445 and the Advanced Combustion Engineering Research Center at the University of Utah and Brigham Young University.

References

[1]Seinfeld, J. H., *Atmospheric Chemistry and Physics of Air Pollution*, Wiley, New York, 1986.

[2]Bahr, D. W., "Gas Turbine Engine Emission Abatement-Status and Needed Advancements," *Gas Turbine Combustor Design Problems*, edited by A. H. Lefebvre, Hemisphere, New York, 1978, pp. 205–224.

[3]Drake, M. C., Correa, S. M., Pitz, R. W., Shyy, W., and Fenimore, C. P., "Superequilibrium and Thermal Nitric Oxide Formation in Turbulent Diffusion Flames," *Combustion and Flame*, Vol. 69, No. 3, 1987, pp. 347–365.

[4]Bowman, C. T., "Kinetics of Pollutant Formation and Destruction in Combustion," *Progress in Energy and Combustion Science*, Vol. 1, No. 1, 1975, pp. 33–45.

[5]Lavoie, G. A., and Schlader, A. F., "A Scaling Study of No Formation in Turbulent Diffusion Flames of Hydrogen Burning in Air," *Combustion Science and Technology*, Vol. 8, Nos. 5,6, 1974, pp. 215–224.

[6]Kent, J. H., and Bilger, R. W., "Turbulent Diffusion Flames," *14th International Symposium on Combustion*, The Combustion Institute, Pittsburgh, PA, 1973, pp. 615–625.

[7]Jones, W. P., "Models for Turbulent Flows with Variable Density and Combustion," *Prediction Methods for Turbulent Flows*, edited by W. Kollman, Hemisphere, Washington, DC, 1980, pp. 380–421.

[8]Correa, S. M., "Prediction of an Axisymmetric Combusting Flow," *AIAA Journal*, Vol. 22, No. 1, 1984, pp. 1602–1608.

[9]Swithenbank, J., Turan, A., and Felton, P. G., "Three-Dimensional Two-Phase Mathematical Modeling of Gas Turbine Combustors," *Gas Turbine Combustor Design Problems*, edited by A. H. Lefebvre, Hemisphere, New York, 1978, pp. 249–314.

[10]Pope, S. B., "PDF Methods for Turbulent Reactive Flows," *Progress in Energy and Combustion Science*, Vol. 11, No. 2, 1985, pp. 119–192.

[11]Curl, R. L., "Dispersed Phase Mixing: I. Theory and Effects in Simple Reactors," *AIChE Journal*, Vol. 9, No. 2, 1963, pp. 175–181.

[12]Kerstein, A. R., "Linear Eddy Model of Turbulent Scalar Transport and Mixing," *Combustion Science and Technology*, Vol. 60, 1988, Nos. 4–6, pp. 391–421.

[13]Kerstein, A. R., "Linear Eddy Modeling of Turbulent Transport. Part 6. Microstructure of Diffusive Scalar Mixing Fields," *Journal of Fluid Mechanics*, Vol. 231, 1991, pp. 361–394.

[14]Menon, S., McMurtry, P. A., Kerstein, A. R., and Chen, J. Y., "Prediction of NO_x Production in a Turbulent Hydrogen-Air Jet Flame," *Journal of Propulsion and Power*, Vol. 10, No. 2, 1994, pp. 161–168.

[15]Kerstein, A. R., "Linear Eddy Modeling of Turbulent Transport. Part 4. Structure of Diffusion Flames," *Combustion Science and Technology*, Vol. 81, Nos. 1–3, 1992, pp. 75–96.

[16]Chen, J. Y., and Kollman, W., "Chemical Models for PDF Modeling of Hydrogen-Air Nonpremixed Turbulent Flames," *Combustion and Flame*, Vol. 79, No. 1, 1990, pp. 75–99.

[17]Zeldovich, Y. B., Sadovnikov, P. Y., and Frank-Kamenetskii, D. A., *Oxidation of Nitrogen in Combustion*, Academy of Sciences of USSR, Inst. of Chemical Physics, Moscow–Leningrad, translated by M. Shelef, 1947.

[18]Magre, P., and Dibble, R., "Finite Chemical Kinetic Effects in a Subsonic Turbulent Hydrogen Flame," *Combustion and Flame*, Vol. 73, No. 2, 1988, pp. 195–206.

[19]Chen, J. Y., and Kollman, W., "PDF Modeling and Analysis of Thermal NO Formation in Turbulent Nonpremixed Hydrogen-Air Jet Flames," *Combustion and Flame*, Vol. 88, Nos. 3–4, 1992, pp. 397–412.

[20]Warnatz, J., *Combustion Chemistry*, Springer–Verlag, Berlin, 1984.

[21]Miller, J. A., and Bowman, C. T., "Mechanism and Modeling of Nitrogen Chemistry in Combustion," *Progress in Energy and Combustion Science*, Vol. 15, 1989, p. 287.

[22]Kerstein, A. R., "Linear Eddy Modeling of Turbulent Transport. II: Application to Shear Layer Mixing," *Combustion and Flame*, Vol. 75, 1989, pp. 397–413.

[23]Kerstein, A. R., "Linear Eddy Modeling of Turbulent Transport. Part 3. Mixing and Differential Molecular Diffusion in Jets," *Journal of Fluid Mechanics*, Vol. 216, 1990, pp. 411–435.

[24]Kerstein, A. R., "Linear Eddy Modeling of Turbulent Transport. Part 7. Finite-Rate Chemistry and Multistream Mixing," *Journal of Fluid Mechanics*, Vol. 240, 1992, pp. 289–313.

[25]McMurtry, P. A., Gansauge, T. C., Kerstein, A. R., and Drueger, S. K., "Linear Eddy Simulations of Mixing in a Homogeneous Turbulent Flow," *Physics of Fluids A*, Vol. 5, No. 4, 1993, pp. 1023–1034.

[26]Hartung, H. K., and Hiby, J. W., "Acceleration of Turbulent Mixing in Tubes," *Chemi-Ingeneieur-Technik*, Vol. 18, 1972, pp. 1051–1057.

[27]Breidenthal, R. E., Tong, K., Wong, G. S., Hamerquist, R. D., and Landry, P. B., "Turbulent Mixing in Two-Dimensional Ducts with Transverse Jets," *AIAA Journal*, Vol. 24, No. 11, 1986, pp. 1867–1869.

[28]Barlow, R. S., Dibble, R. W., Chen, J. Y., and Lucht, R. P., "Effect of Damkohler Number on Superequilibrium OH Concentration in Turbulent Nonpremixed Jet Flames," *Combustion and Flame*, Vol. 82, Nos. 3–4, 1990, pp. 235–251.

[29]Bilger, R. W., and Beck, R. E., "Further Experiments on Turbulent Jet Diffusion Flames," *15th International Symposium on Combustion*, The Combustion Institute, Pittsburgh, PA, 1975, pp. 541–552.

[30]Peters, N., and Donnerhack, S., "Structure and Similarity of Nitric Oxide Production in Turbulent Diffusion Flames," *18th International Symposium on Combustion*, The Combustion Institute, Pittsburgh, PA, 1981, pp. 33–42.

[31]Chen, R. H., and Driscoll, J. F., "Nitric Oxide Levels of Jet Diffusion Flames: Effects of Coaxial Air and Other Mixing Parameters," *23rd International Symposium on Combustion*, The Combustion Institute, Pittsburgh, PA, 1990, pp. 281–288.

[32]Golden, E. M., and Menon, S., *Analysis of Scalar PDF Models for Turbulent Nonpremixed Combustion*, AIAA Paper 97-0253, Jan. 1997.